PHOTONICS Research

Fe_3O_4 nanoparticles as a saturable absorber for a tunable *Q*-switched dysprosium laser around 3 μm

Jian Yang,[1] Jiyi Hu,[2] Hongyu Luo,[1] Jianfeng Li,[1,*] Jishu Liu,[2] Xiaohui Li,[2,3] and Yong Liu[1]

[1]State Key Laboratory of Electronic Thin Films and Integrated Devices, School of Optoelectronic Science and Engineering, University of Electronic Science and Technology of China (UESTC), Chengdu 610054, China
[2]School of Physics and Information Technology, Shaanxi Normal University, Xi'an 710119, China
[3]e-mail: lixiaohui0523@163.com
*Corresponding author: lijianfeng@uestc.edu.cn

Received 30 September 2019; revised 18 November 2019; accepted 18 November 2019; posted 19 November 2019 (Doc. ID 378727); published 24 December 2019

We demonstrate for the first time to our knowledge the use of Fe_3O_4 nanoparticles for *Q*-switching a tunable mid-infrared (Mid-IR) Dy^{3+}-doped ZBLAN fiber laser around 3 μm. The *Q*-switcher was fabricated by depositing the prepared Fe_3O_4 nanoparticles solution onto an Au mirror. Its nonlinear optical response was characterized using a mode locked Ho^{3+}/Pr^{3+}-codoped ZBLAN fiber laser at 2.87 μm, and showed a modulation depth of 11.9% as well as a saturation intensity of 1.44 MW/cm^2. Inserting the device into a tunable Dy^{3+}-doped ZBLAN fiber laser, stable *Q*-switched pulses within the tunable range of 2812.4–3031.6 nm were obtained. When tuning the wavelength to 2931.2 nm, a maximum *Q*-switching output power of 111.0 mW was achieved with a repetition rate of 123.0 kHz and a pulse width of 1.25 μs. The corresponding pulse energy was 0.90 μJ. This demonstration suggests that Fe_3O_4 nanoparticles are a promising broadband saturable absorption material for mid-infrared operation.

https://doi.org/10.1364/PRJ.8.000070

1. INTRODUCTION

Q-switching as a versatile technique that can produce high power and energy short pulses has been widely used in remote sensing, range finding, laser processing, and optical communications [1–3]. For the 3 μm mid-infrared spectral region, *Q*-switched pulses have many specific applications, including laser surgery, material processing, and infrared countermeasures. Recent fast development of mid-IR fiber lasers also stimulates the development of compact and robust *Q*-switched laser sources in this band [4]. Generally, *Q*-switching can be divided into active and passive schemes. Compared to the former one that needs a complex externally controlled modulator, the latter one, based on a low-cost and simple saturable absorber (SA), is more attractive. Until now, SAs based on III-V-compound semiconductors are most widely used because of their mature fabrication processes and ability to customize their properties. The well-known semiconductor saturable absorber mirror (SESAM) is a typical example of those [5–7]. Although their success in *Q*-switching and mode locking has been seen at ~3 μm recently [8,9], their fundamental limitations, which include a narrow operation bandwidth and a complicated fabrication process, motivate researchers to find new materials to overcome these drawbacks.

In the last two decades, broadband and cost-effective, low-dimensional materials were intensively studied as a potential replacement for traditional SAs [10,11]. In 2003, the carbon-nanotubes-based one-dimensional (1D) SA was first developed by Set *et al.* [12]. Since then, it has been widely adopted for pulse generation at 1–2 μm [13,14] and recently was used in ~3 μm fiber laser [15]. Gold nanorods (GNRs), another popular 1D material, have generated interest due to their broadband absorption induced by their distinct surface plasmon resonance and used in pulsed fiber lasers at 1–3 μm [16–18]. However, their nonlinear optical response must be tailored by carefully controlling diameters and chirality. The emergence of graphene that has an ultrabroadband feature as a result of its zero-gap structure [19], started the era of 2D materials [20,21]. In 2009, Bao *et al.* first demonstrated a mode-locked Er^{3+}-doped fiber laser at ~1.5 μm using a graphene SA [22]. After that, other 2D materials, such as topological insulators (TIs) [23–25], black phosphorus (BP) [26–28], and transition metal dichalcogenides (TMDs) [29–31], began to attract attention because of their high third-order nonlinearity, strong light–material interaction, ultrafast carrier dynamics and broadband absorption. Wei *et al.* reported the first passively *Q*-switched Er^{3+}-doped ZBLAN fiber laser at ~3 μm based

on graphene [32]. Our group then showed the feasibility of TI as a Q-switcher at ~3 μm in a Ho^{3+}-doped ZBLAN fiber laser [25]. BP was also used for Q-switching and mode locking in ~2.9 μm Ho^{3+}- and ~3.5 μm Er^{3+}-doped ZBLAN fiber lasers, respectively [27,28]. However, these 2D materials have their own defects, which limited their applications to some extent. For example, graphene has a low modulation depth due to the low absorption efficiency (2.3% per layer), making it unsuitable for short Q-switching. TIs have a complex preparation process since they are made up of two different elements. BP is quite unstable due to its ease of oxidation under ambient conditions. The bandgaps of TMDs are so naturally large that they are unavailable for the mid-infrared, although this situation can be changed by introducing a series of defects, which then complicates the preparation. Accordingly, there still remains a strong motivation to pursue other high-performance saturable absorption materials.

Recently, zero-dimensional (0D) forms of the materials such as aluminum oxide (Al_2O_3), bismuth oxide (Bi_2O_3), nickel oxide (NiO), titanium dioxide (TiO_2), zinc oxide (ZnO), and Fe_3O_4 began to attract attention [33–38]. Similar to 1D and 2D materials, they possess large third-order optical nonlinearity, ultrashort recovery time, a broad operation band, excellent thermal stability, and easy preparation. More importantly, they can be prepared more uniformly because of their smaller sizes and more regular shapes, which gives more flexibility to tailor their properties and higher pulse stability. Among them, Fe_3O_4 nanoparticles have been widely researched. As a transition metal oxide and semiconductor, they have a large third-order nonlinear optical susceptibility of $\chi^{(3)} = 4.0 \times 10^{-10}$ esu [39] and a recovery time of 18–30 ps on a slow time scale [40], both of which are important for high-energy Q-switching. The narrow bandgap of 0.3 eV (~4.2 μm) [41] can be tuned by selecting the diameter of the nanoparticles, which is achieved by adjusting the pH and ionic strength of the precipitation medium during preparation [42,43]. Thus, they can potentially be used as a broadband SA from the visible to the mid-infrared. So far, Fe_3O_4 nanoparticles have been used in Q-switched and mode-locked lasers at ~1 μm [44–46], ~1.5 μm [38,47,48–51], and ~2 μm [52–54]. In 2016, Fe_3O_4 nanoparticles were used as an SA in a passively Q-switched Er^{3+}-doped fiber laser at ~1.5 μm by Bai *et al.* [38]. Wang *et al.* applied the material in Q-switching at ~1 μm in a Nd:YVO_4 laser at 1064.34 nm [44]. Koo *et al.* extended it to the 2 μm band and demonstrated passively Q-switched Tm^{3+}/Ho^{3+} codoped and Tm^{3+}-doped fiber lasers at 1.89 μm [52] and 1.94 μm [54], respectively. Multiwavelength operation at ~1 μm [45] and ~1.5 μm [48], and dark soliton generation at ~1.5 μm [49] were also reported. However, until now there have been no demonstrations at longer wavelengths. Currently, ~2.8 μm Er^{3+}- [55–57] and ~2.9 μm Ho^{3+}- [15,25,27,31] doped ZBLAN fiber lasers are the most widely used mid-infrared platforms for pulse generation based on low-dimensional materials. As an alternative, Dy^{3+}-doped ZBLAN fiber can provide a broader emission band from 2.6 to 3.4 μm [58,59], which fully covers the emission bands of both Er^{3+} and Ho^{3+} ions, and is thus being regarded as a promising mid-infrared laser platform. Recently, Majewski *et al.* presented a continuous wave (CW) Dy^{3+}-doped ZBLAN fiber laser pumped at 1.7 μm tunable from 2.8 to 3.4 μm [59]. Fortin *et al.* reported an in-band pumped high power CW Dy^{3+}-doped ZBLAN fiber at 3.24 μm with a record output power of 10.1 W [60]. Using this platform, picosecond and femtosecond mode-locking based on frequency shifted feedback (FSF) [61] and nonlinear polarization rotation (NPR) [62] was reported. Very recently, we built up a tunable passively Q-switched Dy^{3+}-doped ZBLAN fiber tunable from 2.71 to 3.08 μm using PbS nanoparticles [63]. Meanwhile Woodward *et al.* used BP as the SA to demonstrate a passively Q-switched Dy^{3+}-doped ZBLAN fiber laser at 3.04 μm and a tunable actively Q-switched version from 2.97 to 3.23 μm [64].

In this paper, we demonstrate for the first time the use of Fe_3O_4 nanoparticles to Q-switch a tunable Dy^{3+}-doped ZBLAN fiber laser around 3 μm, showing its potential as a broadband saturable absorption material that can work in the mid-IR region. The morphology and nonlinear optical response at 2.87 μm of the SA are characterized. Using this SA, stable Q-switched pulses tunable from 2.81 to 3.03 μm are produced. The output characteristics with the varied pump power and wavelength are also investigated in detail.

2. PREPARATION AND CHARACTERIZATION OF Fe_3O_4 NANOPARTICLES

The Fe_3O_4 nanoparticles (FNOPs) are dispersed as a stable colloidal suspension in an alcohol carrier. Figure 1(a) shows its atomic structure seen from the (–100) crystal plane. Fe_3O_4, in which there are two kinds of iron ions and one oxygen ion, belongs to a cubic system. In the image, yellow, green, and red circles correspond to positive trivalent iron ions, positive divalent iron ions, and negative divalent oxygen ions, respectively. The transmission electron microscopy (TEM) images of the FNOPs sample with different scales are shown in Figs. 1(b) and 1(c), respectively. The low-magnification TEM image as displayed in Fig. 1(b) reveals that the lateral size of the FNOPs is about 15 nm. The high-resolution TEM image shows a clear crystalline lattice spacing 0.42 nm. Figure 1(d) displays the image of X-ray diffractometer (XRD), and we point the three strongest peaks that are used to identify the phase of material corresponding to crystal diffraction faces of the samples [(220), (400), (422)], which indicate the ultrafine nature and small crystallite size of the particles.

Figure 2(a) shows the experimental setup to measure nonlinear absorption. We first built a SESAM passively mode-locked Ho^{3+}/Pr^{3+}-codoped fluoride fiber laser with a similar structure to that in Ref. [8]. This homemade laser source has a center wavelength of 2870 nm, a pulse duration of approximately 20 ps, and a repetition rate of 17.4 MHz. A beam splitter with a measured transmittance/reflectance ratio of 55:45 was placed at an angle of 45° with respect to the optical path. In the transmitted path, the laser was focused on the previously prepared Fe_3O_4-coated CaF_2 substrate with a 20 mm focal length CaF_2 lens. Detector 1 was placed after it to record the power P_1. The reflected path has the same structure, but the CaF_2 substrate was uncoated. Detector 2 was placed after it to record the power P_2 as the reference. To find the focal point of

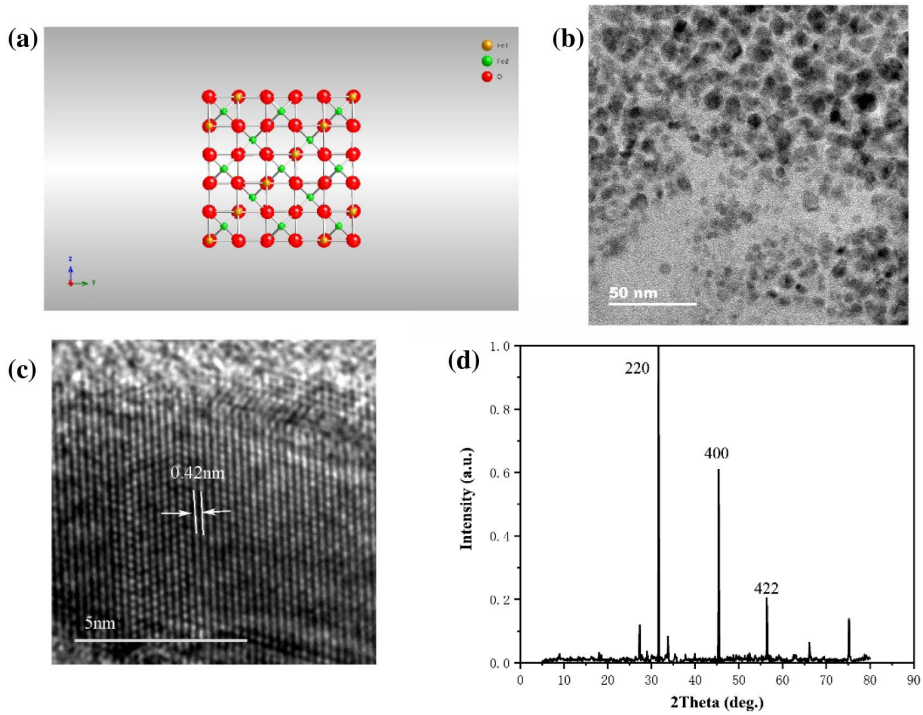

Fig. 1. Characterizations of Fe_3O_4 nanoparticle dispersion: (a) atomic structure, (b) TEM image with a 50 nm scale, (c) HRTEM image with a 5 nm scale, and (d) X-ray diffraction pattern.

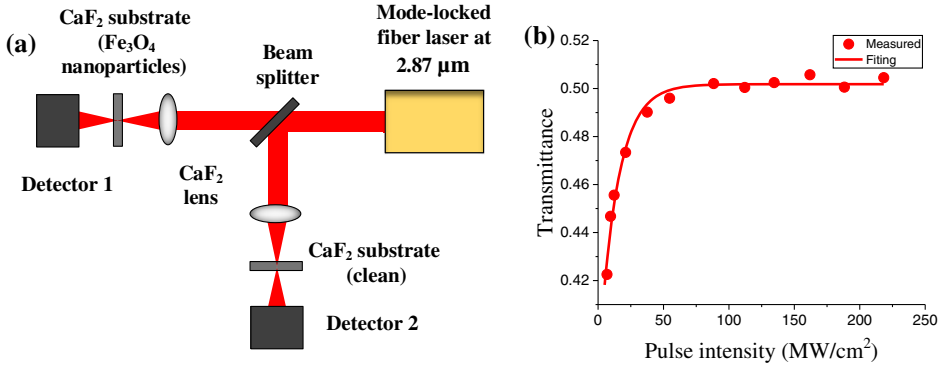

Fig. 2. Nonlinear optical absorption measurement: (a) experimental setup and (b) results at 2.87 μm.

the CaF_2 lens, the Fe_3O_4-coated CaF_2 substrate was moved with a 1D translation stage until the transmitted power P_1 reached a maximum. The transmittance of the Fe_3O_4 sample could be calculated by $45P_1/55P_2$.

We obtain the parameters of the sample by fitting the data with

$$T(I) = 1 - \Delta T \cdot \exp(-I/I_{sat}) - T_{ns}, \quad (1)$$

where $T(I)$ is the intensity-dependent transmittance, ΔT is the modulation depth, I_{sat} is the saturation intensity, and T_{ns} is the nonsaturation loss. The measured nonlinear transmission of the SA fitted based on Eq. (1) is as shown in Fig. 2(b). According to the best fit, ΔT, I_{sat}, and T_{ns} were found to have the values of 11.9%, 14.1 MW/cm^2, and 49.8%, respectively. The modulation depth is lower than most recent mid-infrared SAs made from low-dimensional materials (e.g., TI [36], BP [57], TMDs [31]), but can be tailored by controlling the material thickness. The saturation intensity is also relatively low, which is helpful for initializing pulses.

3. EXPERIMENTAL DESIGN OF THE *Q*-SWITCHED FIBER LASER

Figure 3 shows the experimental setup of our tunable passively *Q*-switched Dy^{3+}-doped ZBLAN fiber laser using Fe_3O_4 nanoparticles SA. The pump source is a homemade CW Yb^{3+}-doped fiber laser at 1.1 μm with a single-mode SMF-28e fiber pigtail. It can yield a maximum output power of 10 W.

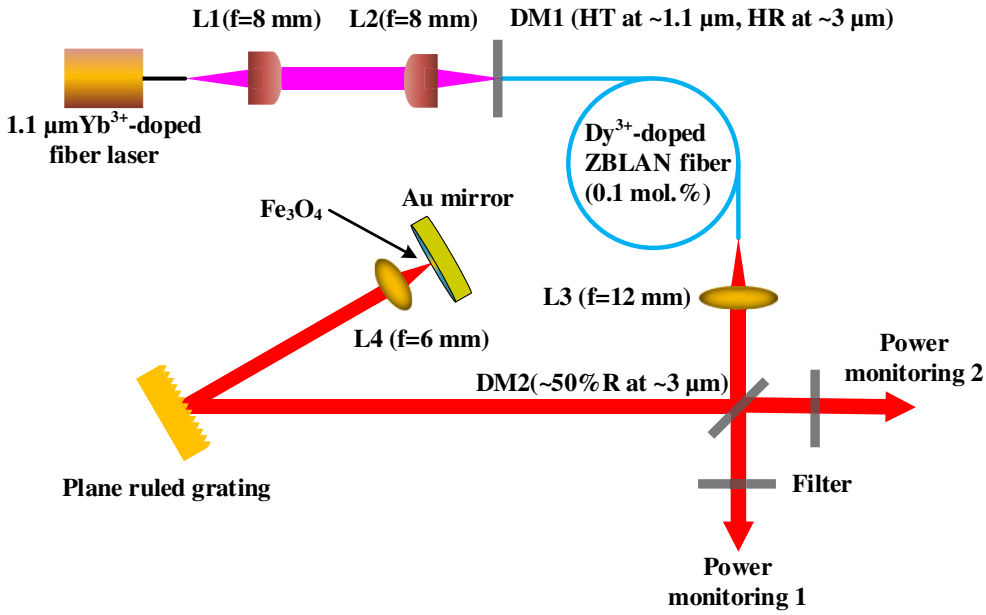

Fig. 3. Experimental setup of the tunable passively Q-switched Dy^{3+}-doped ZBLAN fiber laser using Fe_3O_4 nanoparticles as the SA. L1-L4, four lenses; DM1 and DM2, two dichroic mirrors; HT, high transmittance; HR, high reflectance.

The gain medium is a piece of commercial, single-cladding Dy^{3+}-doped ZBLAN fiber with a core diameter of 15 μm, a cladding diameter of 125 μm, and a cutoff wavelength of 2.55 μm. It has a dopant concentration of 1000 ppm (parts per million) and a length of 1.25 m. The 1.1 μm pump laser was launched into the core of the gain fiber using a pair of aspheric lenses (L1, L2, $f = 8$ mm) (Thorlabs, C240TME-C) with a measured launch efficiency of 88%. DM1 specifically designed with a HT at ~1.1 μm and a HR at ~3 μm was butted against the perpendicularly cleaved fiber pump end as one cavity feedback. The other fiber end was cleaved at an angle of 8° to avoid the parasitic lasing. From that end, the laser was collimated using an anti-reflection (AR) coated objective lens (L3, $f = 12$ mm) (Innovation Photonics, LFO-5-12, 0.13 NA). Following that, DM2 with a reflectance of ~50% at ~3 μm was placed at an angle of 45° with respect to the laser as the output coupler. The reflected beam from this DM was projected onto a plane ruled grating (Thorlabs, 450 lines per mm, blaze wavelength $\lambda_B = 3.1$ μm, blaze angle $\theta_B = 32°$) in a Littman configuration, where the first-order diffracted beam was reflected by the Fe_3O_4 nanoparticles coated Au mirror after focusing using another AR-coated objective lens (Innovation Photonics, LFO-5-6, 0.25 NA). Two commercial bandpass filters (FB3500-500, Thorlabs) were used to purify the output beam. In this scheme, the wavelength could be tuned by rotating the grating. In this process, the distance between L4 and the Au mirror, and the position of L3 were kept aligned to maximize the output due to the chromatic aberrations from L4 and L3. The laser powers were recorded using high-resolution thermal power sensors (Thorlabs, S405C). The temporal pulses were captured using an InAs detector (Judson J12D) with a response time of 2 ns connected with a 500 MHz bandwidth digital oscilloscope. The optical spectrum was measured using a monochromator with a minimum resolution of 0.2 nm (Teledyne Princeton Instruments Acton SP2300). Note that the laser powers mentioned in this paper are all the corrected values according to the transmittance of the used filters.

4. RESULTS

First, the position of the grating was adjusted to maximize the output power of the Q-switched pulses at the launched pump power of 2.89 W and then fixed to study the influence of pump power on the laser output. When the launched pump power was increased to 1.62 W, stable Q-switched pulses were first generated, as shown in Fig. 4(a), with a repetition rate of 49.02 kHz and a pulse width of 2.46 μs. Such a high laser threshold was mainly due to the strong re-absorption of the ground state in the section close to the unpumped fiber end, and also to the high insertion loss of the SA. This stable Q-switching regime could be maintained until the launched pump power reached 2.89 W. The corresponding temporal behavior was recorded, as shown in Fig. 4(b), with an increased repetition rate of 123.0 kHz and a reduced pulse width of 1.25 μs. A further increase of the pump power caused the Q-switched pulses to become unstable and then disappear due to the damage of the SA. At the allowable maximum launched pump power of 2.89 W, the optical and RF spectra were also measured, as shown in Figs. 4(c) and 4(d). The center wavelength was 2932.3 nm, corresponding to the largest gain region of the present cavity. The FWHM of 0.3 nm, which was significantly narrower than in the free-running case [63], resulted from the wavelength selectivity of the grating. The signal-to-noise ratio (SNR) of ~35 dB was typical for stable passive Q-switching [65,66].

Figure 5 shows the evolution of the output Q-switched pulses as a function of the launched pump power. Figure 5(a) shows that the pulse width decreases from 2.46 to 1.25 μs and

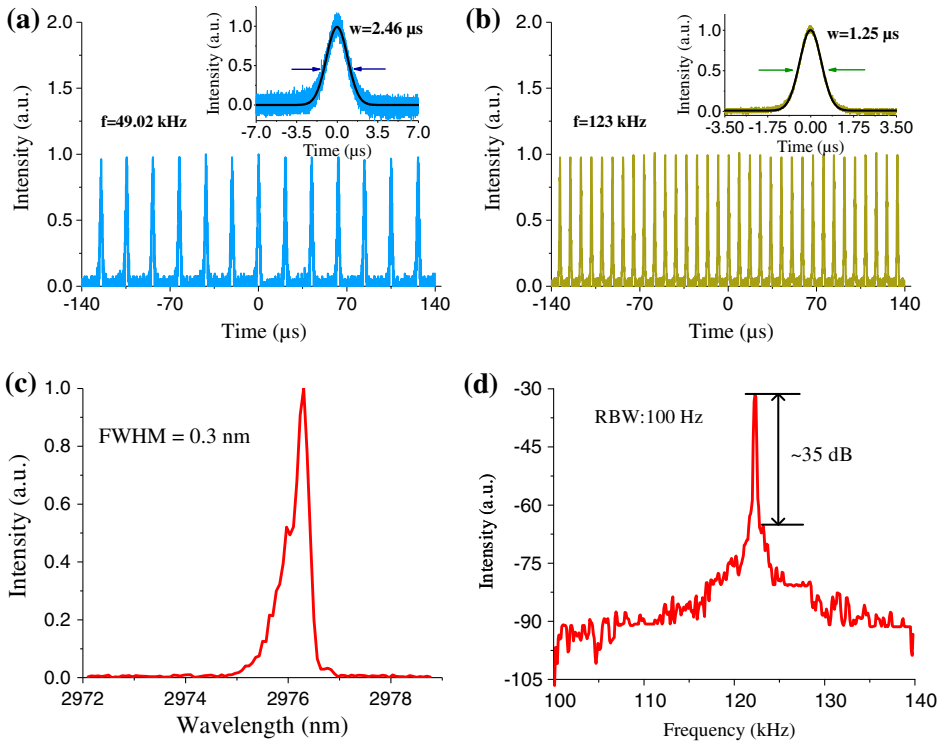

Fig. 4. *Q*-switched pulse train and single pulse waveform (inset) at the launched pump powers of (a) 1.62 W and (b) 2.89 W; (c) optical and (d) RF spectra at the launched pump power of 2.89 W.

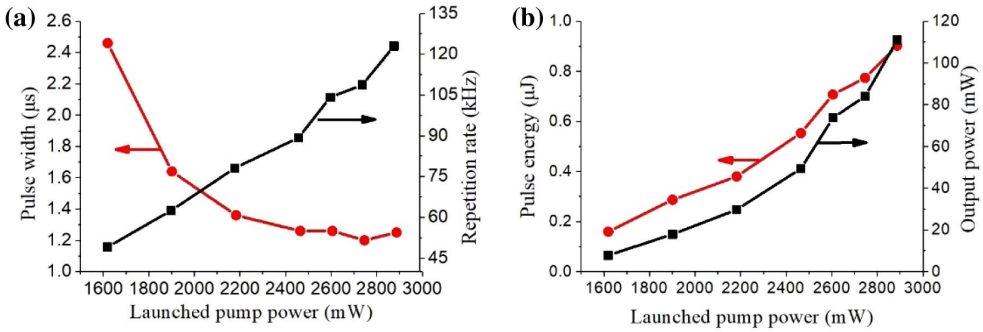

Fig. 5. (a) Pulse width and repetition rate and (b) pulse energy and output power as a function of the launched pump power.

the repetition rate increases from 49.02 to 123.0 kHz when increasing the launched pump power from 1.62 to 2.89 W. These results are in agreement with the standard passive *Q*-switching theory [67,68]. Figure 5(b) shows the variation of the output power and pulse energy over the same pump range. At a launched pump power of 1619.4 mW, the *Q*-switched output power was 7.82 mW, corresponding to a peak power of 0.065 W. Thus, the laser peak intensity on the Au mirror was estimated to be 96.6 MW/cm^2, considering the insertion loss of the objective lens and the diffraction efficiency of the grating, which is larger than the SA saturation intensity. At the maximum launched pump power of 2.89 W, a maximum output power of 111.0 mW with a pulse energy of 0.90 μJ was obtained. The output power fluctuation was measured and calculated to be less than ±2% within 30 min, which indicated its good long-term stability. If the laser was restarted after being off for a long time, however, we needed to slightly align the pump fiber end to make the laser recover to the previous output level.

Then the wavelength tuning of the *Q*-switched laser was performed at a launched pump power of 2.89 W by rotating the ruled plane grating. A wavelength tuning range of 2812.4–3031.6 under *Q*-switching was obtained, as displayed in Fig. 6(a). The output power and pulse energy evolutions with wavelength matched the gain spectrum of the Dy^{3+}-doped ZBLAN fiber [25]. Figure 6(b) shows the repetition rate and pulse width as a function of wavelength. It is seen that the repetition rate first increases and then decreases with the

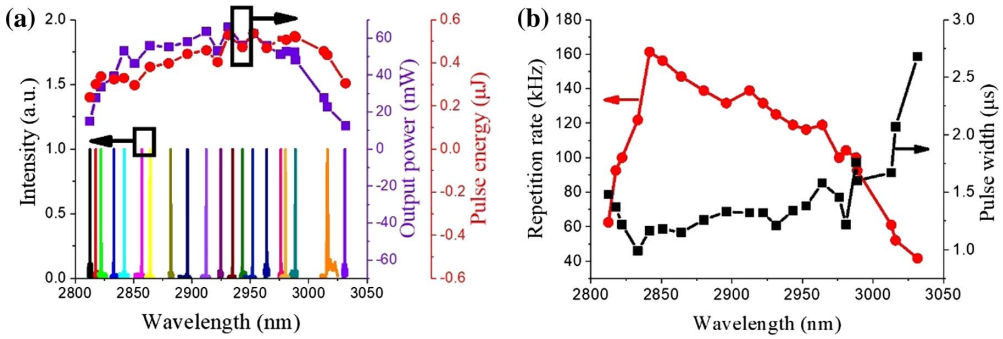

Fig. 6. (a) Output spectrum, output power, and pulse energy, and (b) repetition rate and pulse width as a function of the wavelength at the launched pump power of 2.89 W.

wavelength while the pulse width has an opposite trend. At a wavelength of around 2841.6 nm, the largest repetition rate of 161.3 kHz and shortest pulse width of 790 ns were achieved. These observations are also in agreement with the previously reported tunable passively *Q*-switched fiber lasers in this band [18,25]. After finishing measurements, the laser was placed under ambient condition for one week, during which the laser could always work stably. It indicated good stability of the used Fe_3O_4 nanoparticles.

5. CONCLUSION

In conclusion, we have demonstrated for what we believe is the first time the use of Fe_3O_4 nanoparticles as an efficient broadband mid-IR *Q*-switcher in a tunable Dy^{3+}-doped ZBLAN fiber laser around 3 μm. Stable *Q*-switched pulses were obtained with a tunable wavelength range of 2812.4–3031.6. At a wavelength of 2932.3 nm, a maximum output power of 111.0 mW was obtained with a pulse energy of 0.90 μJ. The corresponding pulse width and repetition rate were 1.25 μs and 123.0 kHz, respectively. This kind of μs pulse laser source after power scaling can find direct applications in the field of laser surgery since its wavelength highly overlaps with the strong absorption region of water [69–72]. The results indicate that Fe_3O_4 nanoparticles are a promising long-term stable SA material under ambient conditions for the mid-infrared region.

Funding. National Natural Science Foundation of China (61421002, 61435003, 61605106, 61722503); Fundamental Research Funds for the Central Universities (ZYGX2019Z012); Joint Fund of Ministry of Education for Equipment Pre-research (6141A02033411); Field Funding for Equipment Pre-research (61404140106, 1114180106A).

REFERENCES

1. P. Rairoux, H. Schillinger, S. Niedermeier, M. Rodriguez, F. Ronneberger, R. Sauerbrey, B. Stein, D. Waite, C. Wedekind, H. Wille, L. Wöste, and C. Ziener, "Remote sensing of the atmosphere using ultrashort laser pulses," Appl. Phys. B **71**, 573–580 (2000).
2. A. Kilpela, J. Ylitalo, K. Maatta, and J. Kostamovaara, "Timing discriminator for pulsed time-of-flight laser rangefinding measurements," Rev. Sci. Instrum. **69**, 1978–1984 (1998).
3. M. Toyoshima, S. Yamakawa, T. Yamawaki, K. Arai, M. R. Garcia-Talavera, A. Alonso, Z. Sodnik, and B. Demelenne, "Long-term statistics of laser beam propagation in an optical ground-to-geostationary satellite communications link," IEEE Trans. Antennas Propag. **53**, 842–850 (2005).
4. S. D. Jackson, "Towards high-power mid-infrared emission from a fiber laser," Nat. Photonics **6**, 423–431 (2012).
5. U. Keller, K. J. Weingarten, F. X. Kartner, D. Kopf, B. Braun, I. D. Jung, R. Fluck, C. Honninger, N. Matuschek, and J. A. der Au, "Semiconductor saturable absorber mirrors (SESAM'S) for femtosecond to nanosecond pulse generation in solid-state lasers," IEEE J. Sel. Top. Quantum **2**, 435–453 (1996).
6. O. G. Okhotnikov, L. Gomes, N. Xiang, T. Jouhti, and A. B. Grudinin, "Mode-locked ytterbium fiber laser tunable in the 980–1070-nm spectral range," Opt. Lett. **28**, 1522–1524 (2003).
7. R. Paschotta, R. Häring, E. Gini, H. Melchior, U. Keller, H. L. Offerhaus, and D. J. Richardson, "Passively *Q*-switched 0.1-mJ fiber laser system at 1.53 μm," Opt. Lett. **24**, 388–390 (1999).
8. J. F. Li, D. D. Hudson, Y. Liu, and S. D. Jackson, "Efficient 2.87 μm fiber laser passively switched using a semiconductor saturable absorber mirror," Opt. Lett. **37**, 3747–3749 (2012).
9. J. F. Li, H. Y. Luo, Y. L. He, Y. Liu, L. Zhang, K. M. Zhou, A. G. Rozhin, and S. K. Turistyn, "Semiconductor saturable absorber mirror passively *Q*-switched 2.97 μm fluoride fiber laser," Laser Phys. Lett. **11**, 065102 (2014).
10. X. F. Liu, Q. B. Guo, and J. R. Qiu, "Emerging low-dimensional materials for nonlinear optics and ultrafast photonics," Adv. Mater. **29**, 1605886 (2017).
11. X. Jiang, S. Gross, M. J. Withford, H. Zhang, D. Yeom, F. Rotermund, and A. Fuerbach, "Low-dimensional nanomaterial saturable absorbers for ultrashort-pulsed waveguide lasers," Opt. Mater. Express **8**, 3055–3071 (2018).
12. S. Y. Set, H. Yaguchi, Y. Tanaka, M. Jablonski, Y. Sakakibara, A. Rozhin, M. Tokumoto, H. Kataura, Y. Achiba, and K. Kikuchi, "Mode-locked fiber lasers based on a saturable absorber incorporating carbon nanotubes," in *Optical Fiber Communications Conference (OFC)* (2003), paper PD44.
13. F. Wang, A. G. Rozhin, V. Scardaci, Z. Sun, F. Hennrich, I. H. White, W. I. Milne, and A. C. Ferrari, "Wideband-tuneable, nanotube mode-locked, fibre laser," Nat. Nanotechnol. **3**, 738–742 (2008).
14. S. Kivistö, T. Hakulinen, A. Kaskela, B. Aitchison, D. P. Brown, A. G. Nasibulin, E. I. Kauppinen, A. Härkönen, and O. G. Okhotnikov, "Carbon nanotube films for ultrafast broadband technology," Opt. Express **17**, 2358–2363 (2009).
15. C. Wei, Y. J. Lyu, H. X. Shi, Z. Kang, H. Zhang, G. S. Qin, and Y. Liu, "Mid-Infrared *Q*-switched and mode-locked fiber lasers at 2.87 μm based on carbon nanotube," IEEE J. Sel. Top. Quantum **25**, 1100206 (2019).
16. Z. Kang, Y. Xu, L. Zhang, Z. X. Jia, L. Liu, D. Zhao, Y. Feng, G. S. Qin, and W. P. Qin, "Passively mode-locking induced by gold nanorods in erbium-doped fiber lasers," Appl. Phys. Lett. **103**, 041105 (2013).

17. J. Lee, J. Koo, J. Lee, and J. H. Lee, "End-to-end self-assembly of gold nanorods in water solution for absorption enhancement at a 1-to-2 μm band for a broadband saturable absorber," J. Lightwave Technol. **34**, 5250–5257 (2016).
18. H. Luo, Z. Kang, Y. Gao, H. Peng, J. Li, G. Qin, and Y. Liu, "Large aspect ratio gold nanorods (LAR-GNRs) for mid-infrared pulse generation with a tunable wavelength near 3 μm," Opt. Express **27**, 4886–4896 (2019).
19. A. K. Geim and K. S. Novoselov, "The rise of graphene," Nat. Mater. **6**, 183–191 (2007).
20. M. S. Xu, T. Liang, M. M. Shi, and H. Z. Chen, "Graphene-like two-dimensional materials," Chem. Rev. **113**, 3766–3798 (2013).
21. F. N. Xia, H. Wang, D. Xiao, M. Dubey, and A. Ramsubramaniam, "Two-dimensional material nanophotonics," Nat. Photonics **8**, 899–907 (2014).
22. Q. L. Bao, H. Zhang, Y. Wang, Z. H. Ni, Y. L. Yan, Z. X. Shen, K. P. Loh, and D. Y. Tang, "Atomic-layer graphene as a saturable absorber for ultrafast pulsed lasers," Adv. Funct. Mater. **19**, 3077–3083 (2009).
23. C. J. Zhao, Y. H. Zou, Y. Chen, Z. T. Wang, S. B. Lu, H. Zhang, S. C. Wen, and B. Y. Tang, "Wavelength-tunable picosecond soliton fiber laser with topological insulator: Bi_2Se_3 as a mode locker," Opt. Express **20**, 27888–27895 (2012).
24. H. Yu, H. Zhang, Y. C. Wang, C. J. Zhao, B. L. Wang, S. C. Wen, H. J. Zhang, and J. Y. Wang, "Topological insulator as an optical modulator for pulsed solid-state lasers," Laser Photon. Rev. **7**, L77–L83 (2013).
25. J. F. Li, H. Y. Luo, L. L. Wang, C. J. Zhao, H. Zhang, H. P. Li, and Y. Liu, "3-μm mid-infrared pulse generation using topological insulator as the saturable absorber," Opt. Lett. **40**, 3659–3662 (2015).
26. Y. Chen, G. B. Jiang, S. Q. Chen, Z. N. Guo, X. F. Yu, C. J. Zhao, H. Zhang, Q. L. Bao, S. C. Wen, D. Y. Tang, and D. Y. Fan, "Mechanically exfoliated black phosphorus as a new saturable absorber for both *Q*-switching and mode-locking laser operation," Opt. Express **23**, 12823–12833 (2015).
27. J. Li, H. Luo, B. Zhai, R. Lu, Z. Guo, H. Zhang, and Y. Liu, "Black phosphorus: a two-dimension saturable absorption material for mid-infrared *Q*-switched and mode-locked fiber lasers," Sci. Rep. **6**, 30361 (2016).
28. Z. P. Qin, T. Hai, G. Q. Xie, J. G. Ma, P. Yuan, L. J. Qian, L. Li, L. M. Zhao, and D. Y. Shen, "Black phosphorus *Q*-switched and mode-locked mid-infrared Er: ZBLAN fiber laser at 3.5 μm wavelength," Opt. Express **26**, 8224–8231 (2018).
29. B. H. Chen, X. Y. Zhang, K. Wu, H. Wang, J. Wang, and J. P. Chen, "*Q*-switched fiber laser based on transition metal dichalcogenides MoS_2, $MoSe_2$, WS_2, and WSe_2," Opt. Express **23**, 26723–26737 (2015).
30. R. Woodward and E. Kelleher, "2D saturable absorbers for fibre lasers," Appl. Sci. **5**, 1440–1456 (2015).
31. C. Wei, H. Luo, H. Zhang, C. Li, J. Xie, J. Li, and Y. Liu, "Passively *Q*-switched mid-infrared fluoride fiber laser around 3 μm using a tungsten disulfide (WS_2) saturable absorber," Laser Phys. Lett. **13**, 105108 (2016).
32. C. Wei, X. S. Zhu, F. Wang, Y. Xu, K. Balakrishnan, F. Song, R. A. Norwood, and N. Peyghambarian, "Graphene *Q*-switched 2.78 μm Er^{3+}-doped fluoride fiber laser," Opt. Lett. **38**, 3233–3236 (2013).
33. S. K. M. Al-Hayali, D. Z. Mohammed, W. A. Khaleel, and A. H. Al-Janabi, "Aluminum oxide nanoparticles as saturable absorber for C-band passively *Q*-switched fiber laser," Appl. Opt. **56**, 4720–4726 (2017).
34. H. Ahmad, S. N. Aidit, and N. Yusoff, "Bismuth oxide nanoflakes for passive *Q*-switching in a C-band erbium doped fiber laser," Infrared Phys. Technol. **95**, 19–26 (2018).
35. A. Nady, M. H. M. Ahmed, A. A. Latiff, A. Numan, C. H. R. Ooi, and S. W. Harun, "Nickel oxide nanoparticles as a saturable absorber for an all-fiber passively *Q*-switched erbium-doped fiber laser," Laser Phys. **27**, 065105 (2017).
36. H. Ahmad, M. A. M. Salim, Z. A. Ali, M. F. Ismail, K. Thambiratnam, A. A. Latif, N. Nayan, and S. W. Harun, "Titanium dioxide-based *Q*-switched dual wavelength in the 1 micron region," Chin. Opt. Lett. **14**, 091403 (2016).
37. H. Ahmad, C. S. J. Lee, M. A. Ismail, Z. A. Ali, S. A. Reduan, N. E. Ruslan, and S. W. Harun, "Tunable *Q*-switched fiber laser using zinc oxide nanoparticles as a saturable absorber," Appl. Opt. **55**, 4277–4281 (2016).
38. X. K. Bai, C. B. Mou, L. X. Xu, S. F. Wang, S. L. Pu, and X. L. Zeng, "Passively *Q*-switched erbium-doped fiber laser using Fe_3O_4-nanoparticle saturable absorber," Appl. Phys. Express **9**, 042701 (2016).
39. T. Hashimoto, T. Yamada, and T. Yoko, "Third-order nonlinear optical properties of sol-gel derived α-Fe_2O_3, γ- Fe_2O_3, and Fe_3O_4 thin films," J. Appl. Phys. **80**, 3184–3190 (1996).
40. G. Xing, J. Jiang, J. Y. Ying, and W. Ji, "Fe_3O_4-Ag nanocomposites for optical limiting: broad temporal response and low threshold," Opt. Express **18**, 6183–6190 (2010).
41. I. Balberg and J. I. Pankove, "Optical measurements on magnetite single crystals," Phys. Rev. Lett. **27**, 596–599 (1971).
42. P. Tartaj, M. del Puerto Morales, S. Veintemillas-Verdaguer, T. Gonzalez- Carreno, and C. J. Serna, "The preparation of magnetic nanoparticles for applications in biomedicine," J. Phys. D **36**, R182–R197 (2003).
43. F. El-Diasty, H. M. El-Sayed, F. I. El-Hosiny, and M. I. M. Ismail, "Complex susceptibility analysis of magneto-fluids: optical band gap and surface studies on the nanomagnetite-based particles," Curr. Opin. Solid State Mater. Sci. **13**, 28–34 (2009).
44. X. Wang, Y. G. Wang, D. Mao, L. Li, and Z. D. Chen, "Passively *Q*-switched Nd:YVO_4 laser based on Fe_3O_4 nanoparticles saturable absorber," Opt. Mater. Express **7**, 2913–2921 (2017).
45. S. K. M. Al-Hayali and A. H. Al-Janabi, "Dual-wavelength passively *Q*-switched ytterbium-doped fiber laser using Fe_3O_4-nanoparticle saturable absorber and intracavity polarization," Laser Phys. **28**, 035103 (2018).
46. L. Li, R. D. Lv, S. C. Liu, Z. D. Chen, J. Wang, Y. G. Wang, W. Ren, and W. J. Liu, "Ferroferric-oxide nanoparticle based *Q*-switcher for a 1 μm region," Opt. Mater. Express **9**, 731–738 (2019).
47. D. Mao, X. Q. Cui, W. D. Zhang, M. K. Li, T. X. Feng, B. B. Du, H. Lu, and J. L. Zhao, "*Q*-switched fiber laser based on saturable absorption of ferroferric-oxide nanoparticles," Photon. Res. **5**, 52–56 (2017).
48. Y. S. Chen, J. D. Yin, H. Chen, J. Z. Wang, P. G. Yan, and S. C. Ruan, "Single-wavelength and multiwavelength *Q*-switched fiber laser using Fe_3O_4 nanoparticles," IEEE Photon. J. **9**, 1501009 (2017).
49. L. Li, Y. G. Wang, X. Wang, R. D. Lv, S. C. Liu, Z. D. Chen, and J. Wang, "Generation of dark solitons in Er-doped fiber laser based on ferroferric-oxide nanoparticles," Opt. Laser Technol. **103**, 354–358 (2018).
50. N. Li, H. Jia, J. X. Liu, L. H. Cui, Z. X. Jia, Z. Kang, G. S. Qin, and W. P. Qin, "Fe_3O_4 nanoparticles as the saturable absorber for a mode-locked fiber laser at 1558 nm," Laser Phys. Lett. **16**, 065102 (2019).
51. H. S. Wang, F. Y. Zhao, Z. J. Yan, X. H. Hu, K. M. Zhou, T. Zhang, W. Zhang, Y. S. Wang, W. Zhao, L. Zhang, and C. D. Sun, "Excessively tilted fiber grating based Fe_3O_4 saturable absorber for passively mode-locked fiber laser," Opt. Express **27**, 15693–15700 (2019).
52. J. H. Koo, J. S. Lee, J. H. Kim, and J. H. Lee, "A *Q*-switched 1.89 μm fiber laser using an Fe_3O_4-based saturable absorber," J. Lumin. **195**, 181–186 (2018).
53. X. Y. Liu, K. J. Yang, S. Z. Zhao, J. Zhao, T. Li, W. C. Qiao, G. Q. Li, D. C. Li, B. T. Zhang, J. L. He, J. T. Bian, L. H. Zheng, L. B. Su, and J. Xu, "Ferroferric-oxide nanoparticle based optical modulator for 2 μm spectral region," IEEE Photon. Technol. Lett. **30**, 777–780 (2018).
54. J. H. Koo, K. H. Jeong, B.-A. Yu, and W. J. Shin, "Evanescent field interaction with Fe_3O_4 nano-particle for passively *Q*-switched thulium-doped fiber laser at 1.94 μm," Opt. Laser Technol. **119**, 105579 (2019).
55. P. H. Tang, Y. Tao, Y. L. Mao, M. Wu, Z. Y. Huang, S. N. Liang, X. H. Chen, X. Qi, B. Huang, J. Liu, and C. J. Zhao, "Graphene/MoS_2 heterostructure: a robust mid-infrared optical modulator for Er^{3+}-doped ZBLAN fiber laser," Chin. Opt. Lett. **16**, 020012 (2018).
56. P. H. Tang, M. Wu, Q. K. Wang, L. L. Miao, B. Huang, J. Liu, C. J. Zhao, and S. C. Wen, "2.8-μm pulsed Er^{3+}:ZBLAN fiber laser modulated by topological insulator," IEEE Photon. Technol. Lett. **28**, 1573–1576 (2016).
57. Z. P. Qin, G. Q. Xie, H. Zhang, C. J. Zhao, P. Yuan, S. C. Wen, and L. J. Qian, "Black phosphorus as saturable absorber for the *Q*-switched Er:ZBLAN fiber laser at 2.8 μm," Opt. Express **23**, 24713–24718 (2015).

58. L. Gomes, A. F. H. Librantz, and S. D. Jackson, "Energy level decay and excited state absorption processes in dysprosium-doped fluoride glass," J. Appl. Phys. **107**, 053103 (2010).
59. M. R. Majewski, R. I. Woodward, and S. D. Jackson, "Dysprosium-doped ZBLAN fiber laser tunable from 2.8 μm to 3.4 μm, pumped at 1.7 μm," Opt. Lett. **43**, 971–974 (2018).
60. V. Fortin, F. Jobin, M. Larose, M. Bernier, and R. Vallée, "10-W-level monolithic dysprosium-doped fiber laser at 3.24 μm," Opt. Lett. **44**, 491–494 (2019).
61. R. I. Woodward, M. R. Majewski, and S. D. Jackson, "Mode-locked dysprosium fiber laser: picosecond pulse generation from 2.97 to 3.30 μm," APL Photon. **3**, 116106 (2018).
62. Y. H. Wang, F. Jobin, S. Duval, V. Fortin, P. Laporta, M. Bernier, G. Galzerano, and R. Vallée, "Ultrafast Dy^{3+}: fluoride fiber laser beyond 3 μm," Opt. Lett. **44**, 395–398 (2019).
63. H. Y. Luo, J. F. Li, Y. Gao, Y. Xu, X. H. Li, and Y. Liu, "Tunable passively *Q*-switched Dy^{3+}-doped fiber laser from 2.71 to 3.08 μm using PbS nanoparticles," Opt. Lett. **44**, 2322–2325 (2019).
64. R. I. Woodward, M. R. Majewski, N. Macadam, G. Hu, T. Albrow-Owen, T. Hasan, and S. D. Jackson, "*Q*-switched Dy:ZBLAN fiber lasers beyond 3 μm: comparison of pulse generation using acousto-optic modulation and inkjet-printed black phosphorus," Opt. Express **27**, 15032–15045 (2019).
65. C. Wei, X. S. Zhu, R. A. Norwood, and N. Peyghambarian, "Passively *Q*-switched 2.8-μm nanosecond fiber laser," IEEE Photon. Technol. Lett. **24**, 1741–1744 (2012).
66. T. Zhang, G. Y. Feng, H. Zhang, X. H. Yang, S. Y. Dai, and S. H. Zhou, "2.78 μm passively *Q*-switched Er^{3+}-doped ZBLAN fiber laser based on PLD-Fe^{2+}:ZnSe film," Laser Phys. Lett. **13**, 075102 (2016).
67. Z. Luo, C. Liu, Y. Huang, D. Wu, J. Wu, H. Xu, Z. Cai, Z. Lin, L. Sun, and J. Weng, "Topological-insulator passively *Q*-switched double-clad fiber laser at 2 μm wavelength," IEEE J. Sel. Top. Quantum Electron **20**, 0902708 (2014).
68. H. Yu, X. Zheng, K. Yin, X. Cheng, and T. Jiang, "Nanosecond passively *Q*-switched thulium/holmium-doped fiber laser based on black phosphorus nanoplatelets," Opt. Mater. Express **6**, 603–609 (2016).
69. K. A. Khatri, V. Ross, J. M. Grevelink, C. M. Magro, and R. R. Anderson, "Comparison of erbium:YAG and carbon dioxide lasers in resurfacing of facial rhytides," Arch. Dermatol. **135**, 391–397 (1999).
70. S. Stübinger, J. P. Dissmann, N. C. Pinho, B. Saldamli, O. Seitz, and R. Sader, "A preliminary report about treatment of bisphosphonate related osteonecrosis of the jaw with Er:YAG laser ablation," Lasers Surg. Med. **41**, 26–30 (2009).
71. L. S. Bass, "Erbium:YAG laser skin resurfacing: preliminary clinical evaluation," Ann. Plast. Surg. **40**, 328–334 (1998).
72. S. Karsai, A. Czarnecka, M. Jünger, and C. Raulin, "Ablative fractional lasers (CO_2 and Er:YAG): a randomized controlled double-blind split-face trial of the treatment of peri-orbital rhytides," Lasers Surg. Med. **42**, 160–167 (2010).